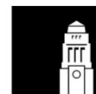

UNIVERSITY OF LEEDS

This is a repository copy of *Composite whey protein–cellulose nanocrystals at oil-water interface: Towards delaying lipid digestion*.

White Rose Research Online URL for this paper:
http://eprints.whiterose.ac.uk/122848/

Version: Accepted Version

Article:

Sarkar, A orcid.org/0000-0003-1742-2122, Li, H, Cray, D et al. (1 more author) (2018) Composite whey protein–cellulose nanocrystals at oil-water interface: Towards delaying lipid digestion. Food Hydrocolloids, 77. pp. 436-444. ISSN 0268-005X

https://doi.org/10.1016/j.foodhyd.2017.10.020

(c) 2017, Elsevier Ltd. This manuscript version is made available under the CC BY-NC-ND 4.0 license https://creativecommons.org/licenses/by-nc-nd/4.0/

Reuse
This article is distributed under the terms of the Creative Commons Attribution-NonCommercial-NoDerivs (CC BY-NC-ND) licence. This licence only allows you to download this work and share it with others as long as you credit the authors, but you can't change the article in any way or use it commercially. More information and the full terms of the licence here: https://creativecommons.org/licenses/

Takedown
If you consider content in White Rose Research Online to be in breach of UK law, please notify us by emailing eprints@whiterose.ac.uk including the URL of the record and the reason for the withdrawal request.

eprints@whiterose.ac.uk
https://eprints.whiterose.ac.uk/

Composite whey protein–cellulose nanocrystals at oil-water interface: Towards delaying lipid digestion

Anwesha Sarkar [1]*, Hancong Li [1], Deborah Cray [1] and Sally Boxall [2]

[1] Food Colloids and Processing Group, School of Food Science and Nutrition, University of Leeds, Leeds LS2 9JT, UK

[2] Bioimaging Facility, Faculty of Biological Sciences, University of Leeds, Leeds LS2 9JT, UK

*Corresponding author:

Dr. Anwesha Sarkar

Food Colloids and Processing Group,

School of Food Science and Nutrition, University of Leeds, Leeds LS2 9JT, UK.

E-mail address: A.Sarkar@leeds.ac.uk (A. Sarkar).

Abstract

Lipid digestion is an interfacial process that is largely controlled by the adsorption of lipase + colipase + bile salts onto the surface of the emulsified lipid droplets. Therefore, engineering oil-in-water (O/W) interfaces that prevent competitive displacement by bile salts and/or delay the transportation of lipase to the hydrophobic lipid core can be effective strategies to delay lipolysis. In this study, we present such an interface using composite protein-particle system, consisting of whey protein isolate (WPI) (1 wt%) + cellulose nanocrystals (CNCs) (1-3 wt%). Droplet size, microscopy at various length scales (confocal, electron microscopy), ζ-potential and kinetics of fatty acid release were used to assess how the presence of CNCs impacted the microstructural stability of the emulsions in in vitro duodenal conditions (pH 6.8, 37 °C). Adding CNCs at sufficiently high concentrations (3 wt%) significantly decreased the rate and degree of lipolysis as compared to that of protein-coated emulsion droplets. The principal cause of this altered lipolysis profile was the binding of bile salts by CNCs, which restricted both the interfacial displacement and solubilization of lipid-digestion products by bile salts. The CNCs can be envisaged to be strongly bound to the protein-coated droplets by virtue of hydrogen bonding with the underlying protein. Furthermore, the ability of the CNCs in the continuous phase to bridge several protein-coated droplets reduced the overall surface area available for the lipolysis. Composite WPI + CNC interface holds promise in designing physiologically relevant emulsions to target satiety or delivery systems for sustained release of lipophilic components.

Keywords

Cellulose nanocrystals, emulsion; particle-protein interface; bile salts; pancreatin

48 # 1 Introduction

49 Obesity is a growing global health crisis, which has more than doubled in extent in the
50 last 25 years. As of 2014, more than 1.9 billion adults were overweight globally, and
51 of those over 600 million people were obese (WHO, 2015). Among many strategies to
52 achieve weight management, food scientists, psychologists and nutritionists are
53 attempting to enhance the satiating and satiety-promoting properties of food in order
54 to generate appetite suppression. In the case of lipids, satiety hormones can be
55 triggered by the presence of undigested lipids in the ileum via the so-called "ileal
56 brake" mechanism (Maljaars, Peters, Mela, & Masclee, 2008). Hence, a delayed lipid
57 digestion in the intestine that will release the lipids in a more sustained manner and
58 has potential to promote the feeling of satiety has become a target of research in the
59 literature.

60 Nearly 70–90% of the lipid digestion takes place in the duodenal i.e. in the upper
61 part of the small intestine in healthy human adults. Lipid digestion is essentially an
62 interfacial process that involves complex adsorption phenomenon of lipase/colipase
63 and bile salts onto the surface of the oil droplets (Sarkar, Ye, & Singh, 2016c; Singh
64 & Sarkar, 2011). Bile salts are bio-surfactants that competitively push out the
65 interfacial materials originally present at the surface, facilitating the adsorption of
66 pancreatic lipase-colipase complex and subsequent lipolysis (Maldonado-Valderrama,
67 Wilde, Macierzanka, & Mackie, 2011). In the last decade two key food-structuring
68 approaches have been investigated to delay intestinal lipolysis, which would allow the
69 detection of undigested lipids in the distal parts of the intestine. The first one involved
70 modulating the interfacial parameters of emulsion (size, charge, interfacial
71 composition etc.) in order to prevent competitive displacement of the original
72 interfacial materials by bile salts and adsorption of lipase thus delaying the process of

73 binding of lipase/colipase complexes to act on the bile-coated oil droplets (Corstens,
74 et al., 2017; Golding, 2014; Golding & Wooster, 2010; Sandra, Decker, &
75 McClements, 2008; Sarkar, Horne, & Singh, 2010c; Sarkar, et al., 2016a). The second
76 approach included restricting the transport of lipase to the emulsified lipid droplets via
77 encapsulation of the emulsion droplets within a gel system (Guo, Bellissimo, &
78 Rousseau, 2017; Guo, Ye, Lad, Dalgleish, & Singh, 2014; Sarkar, et al., 2015). It is
79 now clearly recognized that both ionic surfactants and biopolymers are generally
80 easily displaced from the emulsion droplet surface by bile salts during duodenal
81 digestion (Mackie, Gunning, Wilde, & Morris, 2000; Maldonado-Valderrama, et al.,
82 2011; Sarkar, Horne, & Singh, 2010b; Sarkar, et al., 2016c). However, lately, it has
83 been demonstrated that particle-laden interfaces, such as those created by chitin
84 nanocrystals (Tzoumaki, Moschakis, Scholten, & Biliaderis, 2013), intact or fused
85 whey protein microgel particles (Sarkar, et al., 2016a) were not displaced by bile
86 salts, by virtue of high desorption energy of these particles from the interfaces.
87 One alternative strategy is to coat protein-stabilized interfaces with a layer of
88 particles, which would provide a steric hindrance to the transport of lipase to
89 hydrophobic lipid core. Recently, such protein-particles laden composite interfaces
90 have shown promising effects on enhancing the gastric stability of oil-in-water (O/W)
91 emulsions (Sarkar, Zhang, Murray, Russell, & Boxal, 2017). In this study, cellulose
92 nanocrystal particles (CNCs) were used to create O/W emulsions with composite
93 protein-CNC interfaces by carefully exploiting the electrostatic attraction between
94 cationic whey protein and negatively charged CNCs at pH 3 (Sarkar, et al., 2017). The
95 presence of higher concentration of particles (3 wt%) increased the interfacial shear
96 viscosity of the underlying protein film by almost 40 times and thus, increased the
97 resistance of the interfacial protein film to subsequent rupture by pepsin in the gastric

98 regime at pH 3 (60% intact interfacial protein remained after gastric digestion). The
99 composite WPI-CNC interfacial layer inhibited droplet coalescence in the gastric
100 phase. Such droplet coalescence would have occurred rather spontaneously in an
101 emulsion stabilized by WPI alone, where almost no intact interfacial protein tends to
102 remain after gastric digestion (Sarkar, Goh, & Singh, 2010a; Sarkar, Goh, Singh, &
103 Singh, 2009b; Sarkar & Singh, 2016b; Sarkar, et al., 2017; Singh, et al., 2011).
104 Besides formation of rigid composite interface, the network formation by the CNCs in
105 the bulk (continuous) phase was also hypothesized to reduce the overall kinetics of
106 interfacial proteolysis (Sarkar, et al., 2017).

107 In this study, we have focused on duodenal lipolysis of those emulsions
108 stabilized by composite WPI-CNC interfacial layer, latter created by interfacial
109 electrostatic complexation of mutually complimentarily charged species at pH 3. We
110 hypothesize that the presence of such unmodified CNCs at the WPI-stabilized O/W
111 interface could prevent the competitive displacement by bile salts via steric and/or
112 electrostatic effects and thus might contribute to delaying the lipid digestion. To our
113 knowledge, this is the first study that reports the impact of composite protein-particle
114 laden O/W interface on kinetics of lipid digestion in simulated duodenal conditions.

115

116

2 Materials and Methods

117

2.1 Materials

118 Whey protein isolate (WPI) powder containing 96.3 wt% protein was kindly gifted by
119 Fonterra Limited (Auckland, New Zealand). Cellulose nanocrystal powder (CNC,
120 sulphated) was purchased from CelluForce™, Canada. Sunflower oil was purchased
121 from a local supermarket (Morrisons, UK). Porcine bile extract B8631, porcine
122 pancreatin (P7545, 8 × USP) and sodium azide were purchased from Sigma-Aldrich

123 Company Ltd, Dorset, UK. All other chemicals used were of analytical grade and
124 were obtained from Sigma-Aldrich Chemical Company unless otherwise specified.
125 Milli-Q water having an ionic purity of 18.2 MΩ·cm at 25 °C (water purified by
126 treatment with a Milli-Q apparatus, Millipore Corp., USA) was used for all the
127 experiments.

128

129 2.2 Preparation of emulsions

130 Appropriate quantities of WPI were dispersed in 10 mM citrate buffer solution at pH
131 3 (adjusted using 0.1 M HCl) for 2 h to ensure complete dissolution. Oil-in-water
132 emulsions (20 wt% oil) stabilized by WPI (1 wt%), hereafter cited as W1 were
133 prepared by homogenizing 20.0 wt% sunflower oil and 80.0 wt% WPI solution using
134 two passes through a two-stage valve homogenizer (Panda Plus 2000, GEA Niro
135 Soavi Homogeneizador Parma, Italy) operating at first / second stage pressures of
136 250 / 50 bars, respectively at 25 °C. The maximum temperature reached by the
137 emulsions during the homogenization step was 37 °C. For preparing the protein-
138 particle-stabilized emulsions (schematic diagram shown in Figure 1), the primary
139 emulsions (40 wt% oil, 2 wt% WPI) were dispersed in CNC dispersions (2-6 wt% in
140 citrate buffer at pH 3) (1:1 w/w) to achieve final concentration of 20 wt% oil, 1 wt%
141 WPI and 1 or 3 wt% CNCs, hereafter reported as W1C1 or W1C3, respectively. All
142 the three emulsion samples were prepared in triplicates. Sodium azide (0.02 wt%) was
143 used as a preservative for the emulsions during refrigerated storage at 4 °C.

144

145 2.3 Particle size analysis of emulsions

146 The droplet size distribution of each of the three emulsions before and after duodenal
147 digestion was measured using static light scattering (Malvern MasterSizer 3000,

148 Malvern Instruments Ltd, Malvern, Worcestershire, UK). The absorbance of the
149 emulsion droplets was set to 0.001. Refractive indices of 1.456 and 1.33 were selected
150 for the sunflower oil and the continuous phase, respectively. Mean droplet size was
151 reported as Sauter-average diameter (d_{32}) and volume-average diameter (d_{43})
152 calculated on five measurements on triplicate samples.

153

154 2.4 Zeta-potential

155 The ζ-potential of each of the emulsions before and after duodenal digestion (180
156 minutes) with or without the addition of bile salts and/or pancreatin was measured
157 using a Zetasizer Nano ZS (Malvern Instruments Ltd, Malvern, Worcestershire, UK).
158 Emulsions were diluted to 0.005 wt% droplet concentration in citrate buffer before
159 digestion at pH 3 and simulated duodenal fluid (SDF) buffer after digestion at pH 6.8
160 The samples were equilibrated in respective buffers for 1 h and then were carefully
161 transferred into DTS1070 folded capillary cells to measure the electrophoretic
162 mobility following 30 seconds of equilibration within the equipment. The mobility
163 recorded was then converted to ζ-potential values using classical Smoluchowski
164 equation. Each individual ζ-potential data point was reported as the mean and
165 standard deviation of at least five reported readings made on triplicate samples.

166

167 2.5 Transmission electron microscopy (TEM)

168 Transmission electron microscopy (TEM) was used to gain insights on the size of
169 CNC and interfacial structure of the freshly prepared emulsions. Samples (10 μL)
170 were fixed with 2.5% (v/v) glutaraldehyde, post fixed in 0.1% (w/v) osmium tetroxide
171 and were exposed to serial dehydration in ethanol (20-100%) before being embedded
172 in araldite. Ultra-thin sections (silver-gold 80-100 nm) were then deposited on 3.05

173 mm grids and stained with 8% (v/v) uranyl acetate and lead citrate. The sections were
174 cut on an "Ultra-cut" microtome and imaged using a CM10 TEM microscope
175 (Philips, Surrey, UK).
176
177 2.6 In vitro duodenal digestion
178 For in vitro duodenal digestion, freshly prepared emulsions were diluted with
179 simulated duodenal fluid (SDF) buffer (without or with added bile salts and/or
180 pancreatin) in 1:1 v/v at 37 °C under magnetic stirring at 350 rpm. The SDF
181 was prepared using the harmonized INFOGEST digestion protocol described
182 by Minekus, et al. (2014). The composition of SDF was 0.253 g L^{-1} KCl, 0.054
183 g L^{-1} KH_2PO_4, 3.57 g L^{-1} $NaHCO_3$, 1.12 g L^{-1} NaCl, 0.335 g L^{-1} $MgCl_2(H_2O)_6$,
184 0.44 g L^{-1} $CaCl_2.2H_2O$, 0.23 g L^{-1} bile salts and 125 mg mL^{-1} pancreatin (2800
185 U, 63 U/mL). The temperature was maintained at 37 °C and pH was adjusted to
186 pH 6.8 and equilibrated for 1 h before the addition of pancreatin. Samples of
187 emulsion-SDF mixtures were analysed for size, charge and microstructural
188 changes.
189
190 2.7 Confocal laser scanning microscopy (CLSM)
191 The microstructural changes of the emulsions after in vitro duodenal digestion were
192 imaged using a Zeiss LSM 880 confocal microscope (Carl Zeiss MicroImaging
193 GmbH, Jena, Germany). A small quantity (100 µL) of emulsions after in vitro
194 duodenal digestion in absence and presence of SDF containing bile-pancreatin
195 mixture was mixed with 10 µL each of Nile Red staining oil, Fast Green staining WPI
196 and Calcofluor White staining CNCs for 30 min. The stained samples were then put

197 into custom-made cavity microscopic slides, covered with cover slips and imaged
198 using a 63×/1.4NA oil immersion objective lens.

199

200 2.8 Kinetics of free fatty acid release

201 The free fatty acids (FFAs) generated from emulsified lipids during the digestion of
202 the emulsions in SDF containing bile salts and pancreatin were measured over 3 hours
203 whilst maintaining the pH at 6.8 by addition of NaOH using a pH-Stat (TIM 854,
204 Radiometer). The volume of 0.05 M NaOH consumed was used to calculate the
205 concentration of free fatty acids (FFAs) generated from the triacylglycerols (assuming
206 the generation of 2 FFAs per triacylglycerol molecule by the action of lipase) using
207 Equation 1 (Li & McClements, 2010; Sarkar, et al., 2016a; Sarkar, et al., 2016c):

208

209
210
211
212

$$\%\,FFA = 100 \times \left(\frac{V_{NaOH} \times M_{NaOH} \times M_{W\,Lipid}}{2 \times W_{Lipid}} \right) \quad (1)$$

213

214 The kinetic parameters for the initial FFA release were calculated using
215 Equation (2) (Sarkar, et al., 2016c; Ye, Cui, Zhu, & Singh, 2013):

216

217 $$\ln\left[(\Phi_{max} - \Phi_t)/\Phi_{max}\right] = -kt \quad (2)$$

218

219 where k is the first-order rate constant for FFA release (s^{-1}) and t is the duodenal
220 digestion time (s). The lipolysis half time ($t_{1/2}$, min) i.e. the time required to achieve
221 half lipid digestion and the total FFA level (Φ_{max}, %), were obtained from the FFA
222 curves.

223

224 2.9 Statistical analysis

225 The results were statistically analyzed by analysis of variance (ANOVA) using SPSS
226 software (IBM SPSS Statistics for Windows, Version 22.0. Armonk, NY: IBM Corp)
227 and differences were considered significant when $p < 0.05$ was obtained.

228

229 # 3 Results and discussion

230 3.1 Characteristics of freshly prepared emulsions

231 In this study we briefly introduce the behaviour of aqueous dispersions of
232 CNC particles, which sets the scene for understanding the characteristics of O/W
233 emulsions stabilized by WPI-CNC before and after duodenal digestion. The CNCs
234 used in this study (TEM image, Fig. 1) were crystalline, needle-like in shape with
235 diameter of ~100 nm and high aspect ratio (i.e. the ratio of length to diameter
236 (L/D)) of 10–50. This is in agreement with previous reports on nano-crystalline
237 cellulose where sulfuric acid has been used as a hydrolysing agent (Ehmann, et al.,
238 2013; Sarkar, et al., 2017; Scheuble, Geue, Windhab, & Fischer, 2014).

239 As expected, grafting of numerous sulphate groups (Lin & Dufresne, 2014),
240 which were created in the course of the preparation of these CNCs to remove the
241 amorphous domains, led to significantly high negative surface charges in the CNC
242 dispersion at pH 3. The ζ-potential values were −40 and −44 mV for 1 and 3 wt%
243 CNC, respectively, and displayed higher magnitude of negative charge at pH 6.8
244 (−83 and −89 mV for 1 and 3 wt% CNC, respectively, data not shown). This is
245 consistent with previous reports suggesting that CNCs beared HSO_4^- and SO_4^{2-}
246 surface moieties at near neutral pH and the charge dissociation was almost
247 independent of pH and ionic strength thereafter until pH 10 (Safari, Sheikhi, &
248 van de Ven, 2014).

249 Three emulsions with or without containing CNCs were characterized using
250 droplet size distribution and TEM (Figure 2). The W1 droplets were uniformly
251 distributed in the range of 1-10 µm with $d_{4,3}$ value ≤ 5 μm and the TEM image
252 showed no obvious occurrence of flocculation or coalescence (Figure 2A).
253 However, in presence of CNCs, both W1C1 (Figure 2B) and W1C3 (Figure 2C)
254 showed bimodal and trimodal distributions, respectively with significant
255 population of droplets in the range of 10-100 µm. The second peak in case of both
256 W1C1 and W1C3 were diminished once they were dispersed in 2% SDS (data not
257 shown) suggesting that such larger droplets were corresponding to flocculation of
258 emulsion droplets rather than coalescence, as observed previously (Sarkar, et al.,
259 2017). One might argue that the first peak in the distribution W1C3 is too small (≤
260 0.1 µm) (Figure 2C) to be composed of emulsion droplets, leading us to believe
261 that these were most likely unabsorbed CNCs in the continuous phase. However,
262 such hypothesis must be taken with caution as static light scattering assumes that
263 all species as spherical, whereas CNCs were not spherical as can be observed in
264 Figure 1.

265 The TEM images of the W1C1 and W1C3 (Figures 2B and 2C) revealed
266 interesting information on the presence of CNCs at the O/W interfaces. Both
267 W1C1 and W1C3 showed CNCs at the O/W interface which might be attributed to
268 the electrostatic attractive forces and hydrogen bonding between WPI-coated
269 droplets and CNC (Sarkar, et al., 2017). At lower magnifications, both the W1C1
270 and W1C3 emulsions showed direct evidence of sharing layer of CNC particles
271 between adjacent droplets, supporting bridging phenomenon (Sarkar, Goh, &
272 Singh, 2009a). A closer look at the higher magnification TEM images revealed
273 that in W1C1, the distribution of CNCs at the protein-coated O/W interface

274 seemed to be rather sparse and incomplete. However, in W1C3, a much denser
275 network of CNCs was observed at the droplet interface. This is in line with the
276 higher surface coverage (about 1.4 times) reported in case of 3 wt% as compared
277 to that of 1 wt% CNC (Sarkar, et al., 2017). The cohesion of CNCs forming such a
278 dense network of particles at the W1C3 interface might be attributed to the inter-
279 particle hydrogen bonding, capillary forces and attractive van der Waals forces
280 (Moon, Martini, Nairn, Simonsen, & Youngblood, 2011).

281 It is also worth noting that in W1C3 (lower magnification, Figure 2C), there
282 seemed to be significant level of CNC-CNC aggregation in the continuous phase.
283 First of all, this supports the initial hypothesis of presence of unadsorbed CNCs in
284 the continuous phase as mentioned before in frame of light scattering. Secondly,
285 such CNC-CNC interactions in the continuous phase as well as interactions
286 between CNC adsorbed to the protein-coated droplets and unadsorbed CNCs at the
287 continuous phase might be further attributed to strong intermolecular hydrogen
288 bonds (George & Sabapathi, 2015). The combination of bridging of droplets and
289 CNC-CNC interaction in the continuous phase can reduce the overall surface area
290 of the droplets, and thus can potentially contribute to the slowing down of lipid
291 digestion, latter being largely a surface-area dominated process.

292

293 3.2 Microstructural fate of the emulsions post duodenal digestion

294 The emulsions were digested in an in vitro duodenal model in the presence of ions,
295 bile salts and pancreatin, latter composed of amylase, protease (trypsin) as well as
296 lipase. As can be observed in Figure 3, the droplet size distribution of W1 droplets
297 shifted dramatically after 3 h of duodenal digestion, with significant proportion of the
298 droplets being observed in the size range of 10–100 μm ($p<0.05$). Interestingly, in

299 case of W1C1, there was appearance of another small peak in the range of 100-1000
300 μm. However, in case of W1C3, no such second peak was observed. Irrespective of
301 the original interfacial composition of the emulsions, the $d_{4,3}$ values ranged from 50-
302 60 μm for all the emulsions after duodenal digestion ($p>0.05$), which indicates that
303 the samples were either severely aggregated or had a certain degree of droplet
304 coalescence.

305 To investigate the microstructural behaviour, confocal laser scanning microscopy
306 images were taken at 0-180 min (Figure 4). In the case of W1, droplets underwent
307 strong floc formation at 0 min (absence of pancreatin and bile salts), which clearly
308 suggests the charge screening effects of the Na^{+} and Ca^{2+} ions present in SDF. In
309 presence of pancreatin and bile salts, individual W1 droplets were coalesced to
310 extremely large oil droplets (Sarkar, et al., 2010c). It therefore appears that the
311 dramatic increase in $d_{4,3}$ values of these emulsions under simulated intestinal digestion
312 was linked to the digestive action of both proteases and lipase within the pancreatin.
313 The action of trypsin might have cleaved the proteinaceous interfacial layer
314 generating peptides, which lacked the cohesiveness of the parent protein layer to
315 prevent droplet coalescence. Furthermore, due to the action of pancreatic lipase,
316 surface-active free fatty acids (FFAs) and mono-acylglycerols (MAGs) were possibly
317 generated at the droplet surfaces. These FFAs and MAGs are known to be
318 comparatively less effective at protecting the oil-in-water emulsion droplets against
319 coalescence as compared to that of a protein film present in the original emulsion
320 (Sarkar, et al., 2010c).

321 In the case of W1C1, the emulsion droplets showed limited aggregation in the
322 presence of SDF (Figure 4). This suggests that the CNC-coated droplets were not
323 severely affected in their microstructural integrity by charge screening or ion binding

324 effects. In the presence of pancreatin and bile salts, there was gradual appearance of
325 large coalesced droplets after 30 min. However, the W1C1 micrograph still showed
326 considerable amounts of intact CNC-coated droplets (blue stained by Calcofluor
327 White) of 5-30 µm diameter at 30 min, the population of which gradually diminished
328 as digestion time progressed to 180 min with subsequent fusion of droplets. This
329 suggests that lipid digestion did occur in W1C1 generating FFAs and MAGs leading
330 to subsequent droplet coalescence, however, it appears that there were few CNC-
331 coated droplets, which remained intact even after 180 min of digestion.

332 The behaviour of W1C3 emulsion in presence of SDF without pancreatin/ bile
333 salts did not show any prominent aggregation behaviour, quite similar to that
334 observed in case of W1C1 (Figure 4). Although W1C3 also showed a small degree of
335 coalesced droplets in presence of pancreatin and bile salts, the majority of the
336 population of emulsion droplets were the ones coated by CNC (10-30 µm) that
337 appeared to retain the microstructural intactness. A closer look at these CNC-coated
338 droplets in case of W1C1 and W1C3 revealed that these were actually not individual
339 droplets coated by CNC, but were rather several small emulsion droplets bridged
340 together in a "raspberry-like" floc, resembling emulsion microgel particles (Torres,
341 Murray, & Sarkar, 2016, 2017; Torres, Tena, Murray, & Sarkar, 2017). This indicates
342 that this relatively large fraction of droplets, which were rather encapsulated by and
343 within a CNC particulated layer (3 wt%) might not have had direct access to be
344 cleaved by the enzymes and thus the coalescence was rather diminished in case of
345 W1C3 (Figure 4).

346

347 3.3 ζ-potential

348 To provide indirect quantitative insights into the droplet behaviour, *ζ*-potential
349 values are reported at pH 3 (freshly prepared emulsions), pH 6.8 (pH of SDF) and in
350 presence of SDF without/with the addition of bile salts and/or pancreatin (Figure 5).
351 Freshly prepared W1 droplets were positively charged (~ +41 mV), which is expected
352 as the WPI at the interface was below its isoelectric point (pI) (Sarkar, et al., 2017).
353 However, WPI eventually reversed its charge at pH 6.8, with WPI being above its pI
354 (Sarkar, et al., 2009b). On addition of SDF, W1 showed a strong charge screening
355 effect due to the presence of mono-and divalent cations supporting the microstructural
356 behaviour in Figure 4. In presence of bile salt (Figure 5), W1 showed a rapid rise in
357 magnitude of negative charge ($p<0.05$), which might be attributed to the displacement
358 by negatively charged bile salts. It is noteworthy that bile salt-stabilized oil-in-water
359 emulsion has a *ζ*-potential value of nearly -50 mV (Sarkar, et al., 2016c), which
360 suggests that in this study, the original whey protein layer was almost completely
361 displaced by bile salts (~ -48 mV), achieving an almost bile salt-stabilized interface.
362 This is congruent with the previous findings of orogenic displacement of *β*-
363 lactoglobulin network at O/W interface by bile salts using interfacial measurements
364 and atomic force microscopy (Maldonado-Valderrama, et al., 2008). In addition,
365 gradual increase of negative charge as well as desorption of *β*-lactoglobulin from the
366 O/W interface to the continuous phase in presence of bile salts observed using SDS-
367 PAGE support such bile salts-mediated competitive displacement (Sarkar, et al.,
368 2010b; Sarkar, et al., 2016c). In presence of bile salts and pancreatin, W1 showed
369 significant rise in negative surface charge, which might be attributed to the generation
370 of FFAs and MAGs at the interface, supporting the laser diffraction data (Figure 3)
371 and confocal micrographs showing coalesced droplets (Figure 4).

372 At pH 3, W1C1 containing 1 wt% CNC had a substantial reduction of positive
373 charge as compared to that of W1 ($p<0.05$), which might be attributed to the
374 electrostatic binding of anionic CNC to positively charged protein-coated droplets
375 (Figure 5) (Sarkar, et al., 2017). Since, the coverage by CNC at 1 wt% was not
376 sufficiently complete as shown in the TEM image (Figure 2b), the W1C1 did not
377 show a negative charge at pH 3. At pH 6.8, the samples showed a significantly high
378 magnitude of negative charge, which might be attributed to the sulphated CNCs being
379 highly ionized at pH 6.8, as indicated before, and bound to positive patches of WPI
380 coated emulsions. Furthermore, the strong inter-molecular hydrogen bonding between
381 CNCs and WPI (Qazanfarzadeh & Kadivar, 2016) at the interface also might have led
382 to the presence of CNCs at the interface at pH 6.8, where both WPI and CNC were
383 mostly anionic. The salt-induced screening effects were rather negligible in the case
384 of W1C1 ($p>0.05$). The W1C1 showed almost two-times higher negative charge in
385 presence of bile salts as compared to that in presence of SDF ($p<0.05$), which might
386 suggest bile-mediated displacement. The increase in negative charge was substantially
387 high in the presence of pancreatin, supporting the release of lipid digestion products,
388 such as FFAs and MAGs supporting the coalescence behaviour (Figure 4).

389 The W1C3 was originally negatively charged (Figure 5) due to rather higher
390 coverage of anionic CNC at the WPI-coated droplet surface (Figure 2C, TEM image).
391 At pH 6.8 and in presence of SDF containing no bile salts or pancreatin, the W1C3
392 showed similar behaviour with accumulation of negative charges when compared to
393 W1C1. Interestingly, W1C3 had no change in ζ-potential value after treatment with
394 bile salts ($p>0.05$). These results suggest that bile salts might not have been able to
395 displace completely the thick viscous layer of CNC particles from the WPI-coated
396 interface supporting our hypothesis. Another possibility might be that the CNC

397 particles were highly negatively-charged and retarded the anionic bile salts from the
398 vicinity of the interface. However, one might argue that SDS was able to displace the
399 CNCs from the interface as mentioned in the light scattering data above, but the
400 displacement by bile salts in case of 3 wt% CNC appeared to be rather restricted. This
401 can be explained based on structural differences between SDS and bile salts. In case
402 of bile salts, instead of the classical hydrophilic head–hydrophobic tail geometry like
403 SDS, bile salts have a flat steroidal structure with four rings attached to a short and
404 flexible tail (Vila Verde & Frenkel, 2016). The hydrophilic character of one of the
405 steroid faces arises from the presence of two or three hydroxyl groups. It is highly
406 plausible that CNCs were sequestering bile salts via hydrogen bonding with these
407 hydrophilic groups and thus the interfacial displacement by bile salts were rather
408 restricted. Such sequestering of bile salts by dietary fibres has been previously
409 reported as one of the key mechanism behind the hypercholesteremic properties of
410 dietary fibres (Vahouny, Tombes, Cassidy, Kritchevsky, & Gallo, 1980).

411 In presence of pancreatin, W1C3 droplets became more negatively charged
412 ($p<0.05$). However, it is worth recognizing that the $|\Delta\zeta|$-potential i.e. the difference
413 in magnitude between ζ-potential of samples containing bile salts-pancreatin and bile
414 salts alone was significantly less in W1C3 (6.22 mV) as compared to W1C1 (13.9
415 mV) and W1 (18.1 mV), which might justify the limited degree of droplet
416 coalescence in W1C3 (Figure 4).

417

418 3.4 Kinetics of lipid digestion

419 The lipolysis profiles of the emulsions were assessed in the presence of bile salts
420 and pancreatin using a pH-stat method as shown in Figure 6. As expected, in W1,
421 there was steep rise in FFA release with half of the digestion achieved within the first

422 4 min (Table 1). The W1 generated approximately 46% of FFAs derived from the
423 long-chain FFAs from sunflower oil, which tend to assemble at the oil−water
424 interface and impede further lipid digestion as can be observed by the plateau. In the
425 case of W1C1, the shape of the kinetic plot showed a slight tendency to shift towards
426 the right (Figure 6) leading to a significant decrease in rate and extent of digestion
427 ($p<0.05$) with more than doubled $t_{1/2}$ as compared to that of W1 emulsion (Table 1).

428 The W1C3 containing 3 wt% CNC showed a dramatic decrease in the rate (i.e. k_{lip}
429 and $t_{1/2}$ ~ 8-times lower) and degree of lipid digestion (i.e. ϕ ~ 3-times lower) as
430 compared to W1. This suggests that higher concentration of CNC was capable of
431 forming a rather rigid network at the interface and was not completely displaced by
432 bile salts. The second mechanism can be that higher concentrations of CNCs was
433 capable of sequestering bile salts as discussed above. This might have partially
434 hindered the action of the lipase–colipase complex via restricting its transport to the
435 close proximity of the emulsified lipids, although lipid digestion was not completely
436 prevented.

437 It is well known that the interfacial process of lipolysis involves two key roles of
438 bile salts: anchoring of the bile salt–lipase/colipase complex to the oil/water interface
439 as well as solubilisation of these lipolytic products to continue the digestion (Singh, et
440 al., 2011). Besides restricted interfacial displacement by bile salts as discussed before,
441 the insufficient amount of bile salts (due to CNC-mediated sequestering) available for
442 solubilisation and removal of inhibitory digestion products (e.g. FFAs, mono- and/or
443 di-acylglycerols) also cannot be ignored. Accumulation of such lipolysis inhibitory
444 products at the interface might also have impeded further hydrolysis of the emulsified
445 lipids by pancreatin.

446 Interestingly, in spite of such proposed sequestering of bile salts by CNCs, lipid
447 digestion took place with release of 16% FFA. It should be recognized that CNCs are
448 needle-shaped particles with high aspect ratio, hence close packing cannot be
449 achieved and one can expect relatively large gaps in between the CNC particles. This
450 justifies that lipid digestion still took place as lipase-colipase complex (2.5 nm) could
451 easily squeeze in through such gaps reaching the O/W interface and initiated lipolysis
452 (Sarkar, et al., 2016a). As these droplets were not completely bile-coated and the
453 digestion products were not continuously solubilised by bile salts due to binding by
454 CNCs, the lipolysis was eventually delayed. Furthermore, the reduced surface area of
455 the W1C3 droplets due to the floc formation bridging several droplets together would
456 have significantly reduced the available surface area for the lipolytic enzymes to bind
457 further contributing to the reduction in the rate of lipid digestion.
458

459 ## Conclusions

460 In this study, we demonstrated that it is possible to alter the lipolysis rate by creating a
461 composite interfacial layer with WPI and CNCs, latter formed via electrostatic
462 attraction and hydrogen bonding. The presence of WPI with higher concentration of
463 CNCs (3 wt%) can act as a steric and possibly electrostatic barrier to the displacement
464 by bile salts. The presence of insufficient bile salts for solubilisation of lipolysis end-
465 products due to sequestering of bile salts by CNCs also impeded the degree of
466 lipolysis. Furthermore, the substantial lowering of surface area in W1C3 due to the
467 CNC bridging several emulsion droplets together, almost encapsulating them within
468 CNC-shells led to delaying the digestion of lipids in an in vitro duodenal model.
469 These results together with future in vivo validation realization of such delaying lipid
470 digestion might have potential implications in the designing of physiologically

471 relevant emulsions, for targeting satiety. These composite protein-particle interfaces
472 might be also useful in designing delivery vehicles for lipophilic drugs and bioactive
473 nutrients, where sustained release of lipids is a key requirement.
474
475

Acknowledgements

The authors would like to gratefully acknowledge the contributions of Martin Fuller for his technical support in electron microscopy at the Electron Microscopy Facility within the Astbury Biostructure laboratory, Faculty of Biological Sciences. Author (AS) wishes to thank Professor Brent Murray for useful discussions regarding the complexation of WPI and CNC at the interface and Dr. Melvin Holmes for valuable suggestions regarding the kinetics of lipid conversion as well as curve fitting. The Zeiss LSM880 microscope used in this work was funded by the Wellcome Trust multi-user equipment award WT104918MA.

488 ## References

489 Corstens, M. N., Berton-Carabin, C. C., Kester, A., Fokkink, R., van den Broek, J.
490 M., de Vries, R., Troost, F. J., Masclee, A. A. M., & Schroën, K. (2017).
491 Destabilization of multilayered interfaces in digestive conditions limits their
492 ability to prevent lipolysis in emulsions. Food Structure, 12, 54-63.

493 Ehmann, H. M. A., Spirk, S., Doliška, A., Mohan, T., Gössler, W., Ribitsch, V.,
494 Sfiligoj-Smole, M., & Stana-Kleinschek, K. (2013). Generalized indirect
495 fourier transformation as a valuable tool for the structural characterization of
496 aqueous nanocrystalline cellulose suspensions by small angle x-ray scattering.
497 Langmuir, 29(11), 3740-3748.

498 George, J., & Sabapathi, S. N. (2015). Cellulose nanocrystals: synthesis, functional
499 properties, and applications. Nanotechnology, Science and Applications, 8, 45-
500 54.

501 Golding, M. (2014). Chapter 5 - exploring the relationship between fat surface area
502 and lipid digestibility. In Food Structures, Digestion and Health (pp. 145-
503 167). San Diego: Academic Press.

504 Golding, M., & Wooster, T. J. (2010). The influence of emulsion structure and
505 stability on lipid digestion. Current Opinion in Colloid & Interface Science,
506 15(1), 90-101.

507 Guo, Q., Bellissimo, N., & Rousseau, D. (2017). Role of gel structure in controlling
508 in vitro intestinal lipid digestion in whey protein emulsion gels. Food
509 Hydrocolloids, 69, 264-272.

510 Guo, Q., Ye, A., Lad, M., Dalgleish, D., & Singh, H. (2014). Behaviour of whey
511 protein emulsion gel during oral and gastric digestion: effect of droplet size.
512 Soft Matter, 10(23), 4173-4183.

513 Li, Y., & McClements, D. J. (2010). New mathematical model for interpreting ph-stat
514 digestion profiles: Impact of lipid droplet characteristics on in vitro
515 digestibility. Journal of Agricultural and Food Chemistry, 58(13), 8085-8092.

516 Lin, N., & Dufresne, A. (2014). Surface chemistry, morphological analysis and
517 properties of cellulose nanocrystals with gradiented sulfation degrees.
518 Nanoscale, 6(10), 5384-5393.

519 Mackie, A. R., Gunning, A. P., Wilde, P. J., & Morris, V. J. (2000). Orogenic
520 displacement of protein from the oil/water interface. Langmuir, 16(5), 2242-
521 2247.

522 Maldonado-Valderrama, J., Wilde, P., Macierzanka, A., & Mackie, A. (2011). The
523 role of bile salts in digestion. Advances in Colloid and Interface Science,
524 165(1), 36-46.

525 Maldonado-Valderrama, J., Woodward, N. C., Gunning, A. P., Ridout, M. J.,
526 Husband, F. A., Mackie, A. R., Morris, V. J., & Wilde, P. J. (2008). Interfacial
527 characterization of β-lactoglobulin networks: Displacement by bile salts.
528 Langmuir, 24(13), 6759-6767.

529 Maljaars, P. W. J., Peters, H. P. F., Mela, D. J., & Masclee, A. A. M. (2008). Ileal
530 brake: A sensible food target for appetite control. A review. Physiology &
531 Behavior, 95(3), 271-281.

532 Minekus, M., Alminger, M., Alvito, P., Ballance, S., Bohn, T., Bourlieu, C., Carriere,
533 F., Boutrou, R., Corredig, M., Dupont, D., Dufour, C., Egger, L., Golding, M.,
534 Karakaya, S., Kirkhus, B., Le Feunteun, S., Lesmes, U., Macierzanka, A.,
535 Mackie, A., Marze, S., McClements, D. J., Menard, O., Recio, I., Santos, C.
536 N., Singh, R. P., Vegarud, G. E., Wickham, M. S. J., Weitschies, W., &
537 Brodkorb, A. (2014). A standardised static in vitro digestion method suitable
538 for food - an international consensus. Food & Function, 5(6), 1113-1124.

539 Moon, R. J., Martini, A., Nairn, J., Simonsen, J., & Youngblood, J. (2011). Cellulose
540 nanomaterials review: structure, properties and nanocomposites. Chemical
541 Society Reviews, 40(7), 3941-3994.

542 Qazanfarzadeh, Z., & Kadivar, M. (2016). Properties of whey protein isolate
543 nanocomposite films reinforced with nanocellulose isolated from oat husk.
544 International Journal of Biological Macromolecules, 91, 1134-1140.

545 Safari, S., Sheikhi, A., & van de Ven, T. G. M. (2014). Electroacoustic
546 characterization of conventional and electrosterically stabilized
547 nanocrystalline celluloses. Journal of Colloid and Interface Science, 432, 151-
548 157.

549 Sandra, S., Decker, E. A., & McClements, D. J. (2008). Effect of interfacial protein
550 cross-linking on the in vitro digestibility of emulsified corn oil by pancreatic
551 lipase. Journal of Agricultural and Food Chemistry, 56(16), 7488-7494.

552 Sarkar, A., Goh, K. K. T., & Singh, H. (2009a). Colloidal stability and interactions of
553 milk-protein-stabilized emulsions in an artificial saliva. Food Hydrocolloids,
554 23(5), 1270-1278.

555 Sarkar, A., Goh, K. K. T., & Singh, H. (2010a). Properties of oil-in-water emulsions
556 stabilized by β-lactoglobulin in simulated gastric fluid as influenced by ionic
557 strength and presence of mucin. Food Hydrocolloids, 24(5), 534-541.

558 Sarkar, A., Goh, K. K. T., Singh, R. P., & Singh, H. (2009b). Behaviour of an oil-in-
559 water emulsion stabilized by β-lactoglobulin in an in vitro gastric model. Food
560 Hydrocolloids, 23(6), 1563-1569.

561 Sarkar, A., Horne, D. S., & Singh, H. (2010b). Interactions of milk protein-stabilized
562 oil-in-water emulsions with bile salts in a simulated upper intestinal model.
563 Food Hydrocolloids, 24(2), 142-151.

564 Sarkar, A., Horne, D. S., & Singh, H. (2010c). Pancreatin-induced coalescence of oil-
565 in-water emulsions in an in vitro duodenal model. International Dairy
566 Journal, 20(9), 589-597.

567 Sarkar, A., Juan, J.-M., Kolodziejczyk, E., Acquistapace, S., Donato-Capel, L., &
568 Wooster, T. J. (2015). Impact of protein gel porosity on the digestion of lipid
569 emulsions. Journal of Agricultural and Food Chemistry, 63(40), 8829-8837.

570 Sarkar, A., Murray, B., Holmes, M., Ettelaie, R., Abdalla, A., & Yang, X. (2016a). In
571 vitro digestion of Pickering emulsions stabilized by soft whey protein
572 microgel particles: influence of thermal treatment. Soft Matter, 12(15), 3558-
573 3569.

574 Sarkar, A., & Singh, H. (2016b). Emulsions and foams stabilised by milk proteins. In
575 P. L. H. McSweeney & J. A. O'Mahony (Eds.), Advanced Dairy Chemistry:
576 Volume 1B: Proteins: Applied Aspects (pp. 133-153). New York, NY:
577 Springer New York.

578 Sarkar, A., Ye, A., & Singh, H. (2016c). On the role of bile salts in the digestion of
579 emulsified lipids. Food Hydrocolloids, 60, 77-84.

580 Sarkar, A., Zhang, S., Murray, B., Russell, J. A., & Boxal, S. (2017). Modulating in
581 vitro gastric digestion of emulsions using composite whey protein-cellulose
582 nanocrystal interfaces. Colloids and Surfaces B: Biointerfaces, 158, 137-146.

583 Scheuble, N., Geue, T., Windhab, E. J., & Fischer, P. (2014). Tailored interfacial
584 rheology for gastric stable adsorption layers. Biomacromolecules, 15(8), 3139-
585 3145.

586 Singh, H., & Sarkar, A. (2011). Behaviour of protein-stabilised emulsions under
587 various physiological conditions. Advances in Colloid and Interface Science,
588 165(1), 47-57.

589 Torres, O., Murray, B., & Sarkar, A. (2016). Emulsion microgel particles: Novel
590 encapsulation strategy for lipophilic molecules. Trends in Food Science &
591 Technology, 55(9), 98-108.

592 Torres, O., Murray, B., & Sarkar, A. (2017). Design of novel emulsion microgel
593 particles of tuneable size. Food Hydrocolloids, 71(10), 47-59.

594 Torres, O., Tena, N. M., Murray, B., & Sarkar, A. (2017). Novel starch based
595 emulsion gels and emulsion microgel particles: Design, structure and
596 rheology. Carbohydrate Polymers, 178(Supplement C), 86-94.

597 Tzoumaki, M. V., Moschakis, T., Scholten, E., & Biliaderis, C. G. (2013). In vitro
598 lipid digestion of chitin nanocrystal stabilized o/w emulsions. Food &
599 Function, 4(1), 121-129.

600 Vahouny, G. V., Tombes, R., Cassidy, M. M., Kritchevsky, D., & Gallo, L. L. (1980).
601 Dietary fibers: V. Binding of bile salts, phospholipids and cholesterol from
602 mixed micelles by bile acid sequestrants and dietary fibers. Lipids, 15(12),
603 1012-1018.

604 Vila Verde, A., & Frenkel, D. (2016). Kinetics of formation of bile salt micelles from
605 coarse-grained Langevin dynamics simulations. Soft Matter, 12(23), 5172-
606 5179.

607 WHO, W. H. O. (2015). Obesity and overweight. Fact sheet N°311.

608 Ye, A., Cui, J., Zhu, X., & Singh, H. (2013). Effect of calcium on the kinetics of free
609 fatty acid release during in vitro lipid digestion in model emulsions. Food
610 Chemistry, 139(1), 681-688.

611